POLITECNICO DI TORINO
Repository ISTITUZIONALE

Practical method for the design of pretensioned fully grouted rockbolts in tunnels

(Article begins on next page)

05 May 2024

1 **A practical method for the design of pre-tensioned fully grouted**

2 **rockbolts in tunnels**

3

4 Masoud Ranjbarnia [1], Ahmad Fahimifar [2], Pierpaolo Oreste [3]

5

6 **Abstract**

7 This paper develops an analytical approach to quantitatively model the efficiency of

8 the pre-tensioning of grouted rockbolts in terms of reduction of tunnel convergence.

9 In this study, the distribution of force along the pre-tensioned fully grouted bolt is

10 calculated by the assumption of a rigid connection between the bolt and the rock

11 mass. A compressive force is then applied to the bolt head on tunnel surface to

12 consider the shear relative displacement between the bolt and the rock mass. The

13 magnitude of this compressive force is found by modeling of bolt boundaries

14 stiffness.

15 Finally, the theoretical proposed approach is simplified to be used for the practical purposes.

16 The results show if the stiff end plate is tightened to the bolt head (complete planner

17 contact), the grouting effect of the pre-tensioned fully grouted bolts on tunnel stability

18 can be neglected.

19

[1] PhD student, E-mail: m.ranjbarnia@aut.ac.ir. Department of Civil and Environmental Engineering, Amirkabir University of Technology (Tehran Polytechnic), Hafez Ave., Tehran, Iran

[2] Professor, Corresponding author, E-mail: fahim@aut.ac.ir. Department of Civil and Environmental Engineering, Amirkabir University of Technology (Tehran Polytechnic), Hafez Ave., Tehran, Iran

[3] Associate professor, E-mail: pierpaolo.oreste@polito.it. Department of Environmental, land and infrastructure Engineering, Politecnico di Torino, Corso Duca degli Abruzzi, 24 – 10129, Torino, Italy

21   **Introduction**

22   The systematic grouted rockbolting is widely used as an effective technique in the

23   design and construction of tunnels. The pre-tensioned rockbolts, which transfer initial

24   compressive pressure to the rock mass in order to increase their performance and

25   efficiency, are one of the best and the most appropriate supporting systems to be used

26   in particular circumstances like delay in the bolt installation.

27   During last three decades, a great number of analytical methods have been developed

28   for the study of passive grouted bolts in tunneling design. In a group of approaches,

29   the obtaining of the engineering properties of reinforced rock mass has been focused

30   e.g. with definition of a dimensionless parameter named as "*bolt density*" (which

31   reflects the relative density of bolts with respect to the opening perimeter) to calculate

32   the improved geo-mechanical properties of rock mass (Indraratna and Kaiser 1990a,b;

33   Osguii and Oreste 2010), with introducing a dimensionless coefficient named as

34   "*ground reinforcement- stiffness*" (the contrast of stiffnesses of ground and rockbolt)

35   to be used as the multipliers to obtain the confinement stress of composite material

36   (Carranza-Torres 2009), with presenting of a formulation for mechanical contribution

37   of the rockbolts based on shear stress on the bolt surface (Bobet and Einstein 2011),

38   with obtaining the elastic properties of the rock-bolt material using the shear-lag

39   method (Bobet 2006), and with assuming the influence of bolting on rock mass as a

40   pressure on the tunnel boundary (Bischoff and Smart 1975), as a fictitious increase of

41   the rock mass cohesion (Grasso et al. 1989), and as an increase of confinement stress

42   within rock mass (Fahimifar and Soroush 2005).

43   On the other hand, in another group of approaches, a comprehensive series of studies

44   have been conducted by assuming that the grouted bolt contributes to rock mass in the

2

45 form of a radial pressure within the influence zone of the rockbolt (Aydan 1989; Peila

46 and Oreste 1995; Oreste and Peila 1996; Li and Stillborg 1999; Cai et al. 2004a, b;

47 Guan et al. 2007; Bobet and Einstein 2011).

48 Unlike the passive grouted bolts, the study of pre-tensioned grouted bolts has not been

49 of high interest so far, and their performance is still quantitatively unknown. A few

50 attempts which were carried out were based on the development of the works

51 originally performed for the passive reinforcements (Carranza-Torres 2009; Fahimifar

52 and Ranjbarnia 2009; Bobet and Einstein 2011). Hence, they have involved great

53 limitations which may cause them to give crude predictions.

54 In order to model the pre-tensioned grouted rockbolts as a systematic support of

55 tunnels (at least for the short-time), the relation between the value of pre-tensioned

56 pressure on the tunnel surface (produced by the pre-tensioned force) and that of the

57 fictitious constrained radial pressure (supplied by the proximity of tunnel face) should

58 be particularly taken into consideration. That is, the progressively advancing tunnel

59 face in front of bolted section leads to diminishing of the fictitious constrained radial

60 pressure to zero and ultimately, the pre-tensioned pressure will only remain. Provided

61 that the value of pre-tensioned pressure on the tunnel surface is greater than the

62 constrained radial pressure, advancement of the tunnel face will not change the

63 stresses within the rock mass around tunnel, and the ultimate load will not be

64 changed. Meanwhile, if the value of pre-tensioned pressure is less than the fictitious

65 constrained radial pressure, the tunnel convergence will again occur immediately after

66 the radial pressure becomes less than the initial value prior to bolt installation.

67 Remarking that above discussion is pertinent to the condition that tunnel convergence

68 merely occurs due to tunnel face advancement (short-term movement).

69   Thus, the above-mentioned analytical approaches for the pre-tensioned grouted

70   rockbolts are not appropriate solution due to either neglecting the relation of the pre-

71   tensioned and the fictitious constrained pressures (Carranza-Torres 2009; Fahimifar

72   and Ranjbarnia 2009) or considering constant bolt tensioning (Bobet and Einstein

73   2011).

74   In an effort to bridge this apparent gap in the available methods and tools for analysis

75   of reinforced tunnel by the pre-tensioned grouted rockbolts, this paper develops an

76   analytical approach to quantitatively model the efficiency of the pre-tensioning of

77   grouted rockbolts in terms of reduction of both tunnel convergence.

78   The distribution of force along the bolt is an important issue. In general, the bolt axial

79   force is originated by the relative shear displacements between the bolt and the rock

80   mass which itself affected by both the shear stiffness and the bolt boundaries

81   conditions. Some of the previously mentioned works have obtained the axial force

82   along the bolt e.g. with modeling of shear stress between the bolt and the rock mass,

83   and then integrating of the corresponding function (Li and Stillborg 1999), with

84   considering the constitutive deformation between the bolt and rock mass, and taking

85   derivation to obtain the differential equation of axial force (Cai et al. 2004a, b). In

86   these efforts, the boundary conditions were not taken into account i.e. the force on the

87   tunnel wall was considered zero. Meanwhile; by the in-situ measurements and the

88   results of numerous numerical calculations, Oreste (2008) presented a simple two-line

89   graphic for distribution of axial force along the bolt in which the force on tunnel wall

90   is considered for the stiff end plate.

91   All these works have been carried out for the passive bolts while no attempt has been

92   performed for the pre-tensioned grouted types. Hence, in this paper, a new

93   methodology is also presented to compute the distribution of the force along the pre-

4

94 tensioned grouted bolts. For this purpose, it is calculated by the assumption of a rigid

95 connection between the bolt and the rock mass. A compressive force is then applied to

96 the bolt head on tunnel surface (near boundary) to reduce the bolt force. The

97 magnitude of this compressive force is dependent upon the near boundary condition

98 (i.e. the stiffness of components of nut, washer, and the plate) and the far boundary

99 condition of bolt (i.e. the shear stiffness of the initial anchored length). Therefore,

100 these two boundaries conditions will be also modeled.

101 Finally, as the derived formula of the proposed model is too complicated for practice

102 and preliminary design, a simple method will be introduced with employing the

103 support and the rock mass interaction concepts on the basis of the proposed model.

104

105 **Modeling of systematic pre-tensioned fully grouted bolts**

106 **behavior in tunnels**

107 **General assumptions**

108 A circular tunnel of radius r_i , under plane strain condition, is driven in a

109 homogeneous, isotropic, initially elastic rock mass with a strain-softening behavior

110 subjected to a hydrostatic stress field, p_0.

111 The problem is modeled with the assumption that tunnel closure is only occurred due

112 to advancement of the tunnel face (which is equivalent to the reduction of fictitious

113 radial pressure). Therefore, time-dependent properties of the rock mass are ignored,

114 and short-term convergence of tunnel is only taken into account.

115 As the rockbolts are installed, a certain convergence of tunnel has already been

116 occurred, and an initial plastic zone of radius $\bar{r}_e$ has been developed around the tunnel

117 (Fig. 1a).

118

Theoretical concept of the pre-tensioned grouted rockbolts behavior in

tunnel

The installation process of the pre-tensioned grouted rockbolt, in this paper, consists

of placing a grouted anchor, tensioning the rockbolt and tying end of the bolt by nut

and plate to the tunnel surface, and then grouting the remained of the bolt length.

Once the pre-tensioned force is applied by the plate to tunnel surface, a radial pressure

develops within the rock in the influence domain of itself. Therefore

$$p_{pre-ten} = \frac{T_{pre-ten}}{C_0} \tag{1}$$

where $T_{pre-ten}$ and $p_{pre-ten}$ are the pre-tensioned force and the associated radial

pressure at tunnel surface, respectively. C_0 is the rockbolt effective area at tunnel

surface calculated by

$$C_0 = S_l . S_{c_0} \tag{2}$$

S_l and S_{c_0} are the longitudinal and tangential space of bolts at tunnel surface,

respectively.

The advancement of tunnel face is again restarted after full installation of bolts. Then,

the remained fictitious radial pressure will be further reduced and will be ultimately

diminished. Accordingly, two following different circumstances can occur:

Case A: If the magnitude of the fictitious radial pressure is less than the radial pre-

tensioned pressure, progressive advancement of tunnel face will not result in further

radial displacement (Fig 1a). This is because, due to applying the pre-tensioned

pressure, the remained radial pressure on tunnel surface (after full diminishing of the

fictitious constrained pressure) is greater than the value prior to the bolt installation.

141   Thus, the final bolt force is not greater than the initial applied tension i.e. the bolt

142   force will remain constant along the bolt and will equal to pre-tensioned force. As

143   well, grouting the remained bolt length has no influence on its behavior mechanism

144   but will protect the bolt from corrosion.

145   *Case B*: If the magnitude of the fictitious constrained radial pressure is greater than

146   the pre-tensioned pressure, somewhat re-advancing of tunnel face will lead to further

147   inward radial displacement of the rock mass. So the bolt force will increase till to full

148   diminishing of the fictitious constrained radial pressure, and the plastic radius will

149   become greater (Fig. 1b).

150   Reminding that the magnitude of the pre-tensioned force is a significant fraction of

151   the bolt's yielding capacity so that it does not have a final force to yield.

152

153   **The analytical simulation of the radial pre-tensioned fully grouted bolts**

154   ***Rigid (Ideal) connection between the bolt and rock mass***

155   In general, the grouted rockbolts reinforce and mobilize the inherent strength of the

156   rock mass by offering internal and confining pressure (Huang et al. 2002). Assuming

157   that the bolt contribution is in the form of a radial load spread within its influencing

158   zone, the differential equation of equilibrium for tunnel with circular cross section,

159   uniform in-situ stresses, and close spacing of the rockbolts will be

160
$$\frac{d\sigma_r}{dr} = \frac{\sigma_\theta - \sigma_r}{r} + \frac{dT}{dr}\frac{r_i}{C_0}\frac{1}{r} \tag{3}$$

161   where σ_θ and σ_r are the tangential and radial stresses, respectively. r is a variable

162   showing the radial distance from tunnel center, T is the overall rockbolt tensioned

163   force.

7

164 For *Case A*, as discussed in section 2-2, tunnel convergence will not increase, and the

165 force along the bolt will be almost constant and will equal to the pre-tensioned value

166 i.e. $T = T_{pre-ten}$. Thus, dT/dr will be zero and Eq. (4) will be resulted from Eq. (3)

167 (also by replacing of the Hoek- Brown strength criterion (1980) for rock mass)

168
$$\frac{d\sigma_r}{dr} = \frac{\left[m\sigma_c\sigma_r + s\sigma_c^2\right]^{1/2}}{r}$$
(4)

169 with the following boundary condition

170 (i) At $r = r_i$, $\sigma_r = p_i$ in which $p_{inst} \leq p_i \leq p_0$. (Because, $p_{pre-ten} > p_{inst}$)

171 (ii) At $r = r_e$, $\sigma_r = \sigma_{re}$.

172 where σ_c is uniaxial compressive strength of the intact rock material, and parameters

173 m and s are rock mass constants depending on the nature of the rock mass and its

174 geotechnical conditions. p_i is the magnitude of radial pressure in the tunnel surface,

175 p_{inst} is the fictitious radial pressure induced by the working face at bolt installation

176 time, and σ_{re} is the radial stress at the outer boundary of plastic zone and is obtained

177 by (Hoek and Brown 1980)

178
$$\sigma_{re} = p_0 - M.\sigma_c$$
(5)

179 in which

180
$$M = \frac{1}{2}\left[\left(\frac{m_p}{4}\right)^2 + m_p\frac{p_0}{\sigma_c} + s_p\right]^{1/2} - \frac{m_p}{8}$$
(6)

181 where parameters m_p and s_p are rock mass constants before failure.

182 For *Case B*, dwindling of the radial pressure on tunnel surface from its remained

183 value i.e. p_{inst} to pre-tensioned pressure i.e. $p_{pre-ten}$ leads to increase of radial

184 deformations of rock mass, and imposes further tension to the bolt. Thus, the

8

185   differential equation for this condition will be Eq. (3) with the following boundary

186   conditions

187   (i)   At $r = r_i$, $\sigma_r = p_i$ in which $p_{pre-ten} \leq p_i \leq p_{inst}$

188   (ii)   At $r = r_e$, $\sigma_r = \sigma_{re}$

189   The bolt axial force can be obtained by

$$T = A_b.E_s.\varepsilon_b \tag{7}$$

191   where A_b and E_s are bolt cross section area and the modulus of elasticity of bolt,

192   respectively, and ε_b is the bolt axial strain calculated by

$$\varepsilon_b = \varepsilon_r^{'} + \varepsilon_{pre-ten} \tag{8}$$

194   where $\varepsilon_{pre-ten}$ is the pre-tensioned strain of rockbolts, and ε_r' is the radial strain within

195   rock mass taking place after the bolts installation computed by

$$\varepsilon_r^{'} = \begin{cases} \varepsilon_r - \bar{\bar{\varepsilon}}_r & r_i < r \leq \bar{r}_e \\ \varepsilon_r - \varepsilon_r^e & \bar{r}_e < r \leq r_e \end{cases} \tag{9}$$

197   where ε_r is total radial strain within plastic rock mass, $\bar{\bar{\varepsilon}}_r$ and ε_r^e are the radial strain

198   within the rock mass before the bolts installation in the initial and developed plastic

199   zone, respectively. Reminding that prior to the bolts installation, a plastic

200   displacement in the initial plastic zone, $\bar{r}_e$, and the elastic deformations in the greater

201   plastic zone, r_e, had been developed (Fig. 1b).

202   To solve differential Eqs. (3) and (4), it is essential to employ a numerical method due

203   to their algebraic complexity. For this purpose, Brown et al. (1983) analytical-

204   numerical method with inclusion of the rockbolt parameters is used to calculate

205   stresses and strains around reinforced circular tunnel. This method is an iterative finite

206 difference solution in which the plastic zone is split into annular rings. The

207 differential equation (3) is rewritten for a ring i.e.

$$\frac{\sigma_{r(j-1)} - \sigma_{r(j)}}{r_{(j-1)} - r_{(j)}} = \frac{\left[\dfrac{m_a \sigma_c}{2}\left(\sigma_{r(j)} + \sigma_{r(j-1)}\right) + s_a \sigma_c^2\right]^{1/2}}{\dfrac{r_{(j)} + r_{(j-1)}}{2}} + \frac{T_{(j-1)} - T_{(j)}}{r_{(j-1)} - r_{(j)}} \cdot \frac{r_i}{C_0} \cdot \frac{2}{r_{(j)} + r_{(j-1)}}$$

208

209 (10)

210 in which

$$m_a = \frac{m_{(j-1)} + m_{(j)}}{2} \tag{11}$$

211

$$s_a = \frac{s_{(j-1)} + s_{(j)}}{2}$$

212

213 (12)

214 Manipulating Eq. (10) results the second order equation giving $\sigma_{r(j)}$

$$a \cdot \sigma_{r(j)}^2 + b \cdot \sigma_{r(j)} + c = 0 \tag{13}$$

215

216 and solution is

$$\sigma_{r(j)} = \frac{-b - \sqrt{b^2 - 4ac}}{2a}$$

217

218 For $r_i < r \le \bar{r}_e$ zone

219 $$a = \frac{1}{4K^2} \qquad , \qquad b = -\frac{K_1 - \overline{K}_1}{K} - \frac{\sigma_{r(j-1)}}{2K^2} - 2K_2$$

220 $$c = \sigma_{r(j-1)}\left[\frac{\sigma_{r(j-1)}}{4K^2} + \frac{K_1 - \overline{K}_1}{K} - 2K_2\right] + \left(K_1 - \overline{K}_1\right)^2 - s_a \sigma_c^2$$

221 (14)

222 where

$$\gamma = d\varepsilon_{r(j)} = \varepsilon_{r(j)} - \varepsilon_{r(j-1)} \tag{15}$$

$$224 \qquad K_1 = \frac{A_b E_s r_i}{C_0 \left(r_{(j-1)} - r_{(j)} \right)} \gamma \qquad (16)$$

$$225 \qquad \bar{\gamma} = d\bar{\varepsilon}_{r(j)} = \bar{\varepsilon}_{r(j)} - \bar{\varepsilon}_{r(j-1)} \qquad (17)$$

$$226 \qquad \bar{K}_1 = \frac{A_b E_s r_i}{C_0 \left(r_{(j-1)} - r_{(j)} \right)} \bar{\gamma} \qquad (18)$$

227 and for $\bar{r}_e < r \le r_e$ zone

$$228 \qquad a = \frac{1}{4K^2} \qquad , \qquad b = -\frac{K_1 - K_1^e}{K} - \frac{\sigma_{r(j-1)}}{2K^2} - 2K_2$$

$$229 \qquad c = \sigma_{r(j-1)} \left[\frac{\sigma_{r(j-1)}}{4K^2} + \frac{K_1 - K_1^e}{K} - 2K_2 \right] + \left(K_1 - K_1^e \right)^2 - s_a \sigma_c^2$$

230 \qquad (19)

231 where

$$232 \qquad \gamma^e = d\varepsilon_{r(j)}^e = \varepsilon_{r(j)}^e - \varepsilon_{r(j-1)}^e$$

233 \qquad (20)

$$234 \qquad K_1^e = \frac{A_b E_s r_i}{C_0 \left(r_{(j-1)} - r_{(j)} \right)} \gamma^e \qquad (21)$$

235 After finding the distribution of the stress and strain around circular tunnel, the axial

236 force along the bolt (in the ideal condition) can be obtained by Eq. (7).

237

238 ***Modeling of shear displacement between the bolt and rock mass***

239 To find the bolt force in the reality (to be used in Eq. (10)), the relative shear

240 displacement between the bolt and the rock should be calculated. For this purpose, the

241 following new method is proposed. The force applied through the bolt head deforms

242 the tunnel surface beneath the plate, and the bolt elongation is reduced (Fig. 2). It can

11

243 be said that the reduction of the reinforcement elongation (δ_{rein}) is identical to the

244 deformation of the tunnel surface (Δ_s).

245
$$\left|\Delta_s\right| = \left|\delta_{rein}\right| \tag{22}$$

246 In fact, a portion of the force through the bolt head is devoted for the initial bedding in

247 the components of nut and washer on the plate, bedding of the plate on the rock mass,

248 and compressing of the rock mass. Hence, the force in the bolt head is reduced from

249 T_{max} to T_s. (T_{max} and T_s are the forces through the bolt head in the ideal and the real

250 conditions, respectively).

251 From Eq. (22), it can be written

252
$$\frac{T_s}{K_s} = \frac{T_{rein}}{K_{rein}} \tag{23}$$

253 where K_{rein} is the shear stiffness of the reinforcing element, and K_s describes the

254 equivalent stiffness of the components of nut and washer and the plate's basement.

255 When a stiff end plate tightened to the bolt head (perfect constraint), it is estimated

256 that $K_s \cong (0.5 - 0.8)K_{rein}$ (For the weak rock mass and high in-situ stress, the lower

257 coefficient is used). This is proven in Appendix A (II). However; when a perfect

258 constraint is not guaranteed, the magnitude of K_s is drastically reduced (Oreste 2008)

259 and becomes a very small value. T_{rein} is the magnitude of bolt head force reduction i.e.

260
$$T_{rein} = T_{max} - T_s \tag{24}$$

261 Combining Eq. (23) and Eq. (24), it can be written

262
$$T_s = \frac{K_s}{K_s + K_{rein}} T_{max} \tag{25}$$

263   From above discussion, it can be assumed that T_{rein} acts as a compression force

264   through the bolt head to reduce the bolt elongation and reduces the bolt force from

265   T_{max} to T_s .

266   In the case of the pre-tensioned grouted rockbolts, the computation of the real force

267   applied by the bolt to the tunnel surface may be carried out in two steps as follows:

268   (1)   The computation of the real force due to the pre-tensioned force.

269   (2)   The computation of the real force due to the subsequent load may probably

270   occur after full grouting of the bolt length.

271   For *Case A*, the real force should be only computed due to the pre-tensioned force. As

272   fictitious compression force acts from the bolt head towards the rock mass, the

273   reduction takes place in two sections of the bolt length i.e. in the free length section

274   (un-grouted section) and in the initially anchored length section as observed in Fig.

275   (3).

276 $$\delta_{rein} = \delta_{free} + \delta_{anch} \qquad (26)$$

277   where δ_{free} and δ_{anch} are respectively the reduction of the bolt elongation in the free

278   length and anchored length of the bolt obtained by

279 $$\delta_{free} = \frac{T_{rein}}{K_{free}} \qquad (27)$$

280 $$\delta_{anch} = \frac{T_{rein}}{K_{anch}} \qquad (28)$$

281   in which

282 $$K_{free} = \frac{E_b . A_b}{L_{free}} \qquad (29)$$

13

283
$$K_{anch} = \frac{H}{\lambda} \left(\frac{e^{\lambda L_{anch}} + e^{-\lambda L_{anch}}}{e^{\lambda L_{anch}} - e^{-\lambda L_{anch}}} \right) \tag{30}$$

284 where K_{free} and K_{anch} are the axial stiffness of the free and total anchored length of the

285 bolt for *Case A*, respectively; (See Appendix A (I) for detailed derivation of K_{anch}).

286 L_{free} and L_{anch} are the free and the anchored length of the bolt, and H is a material

287 parameter associates to the shear stiffness between the bolt and the rock mass, and its

288 formulation is available in Appendix A (I). λ is a parameter defined as

289
$$\lambda = \left(\frac{H}{E_{rein}.A_{rein}} \right)^{0.5} \tag{31}$$

290 where A_{rein} and E_{rein} are the area section and the elasticity Modulus of the

291 reinforcement, respectively.

292 Substituting Eqs. (27) and (28) into Eq. (26), and then simplifying gives

293
$$K_{rein}{}^{A} = \frac{K_{free}.K_{anch}}{K_{free} + K_{anch}} \tag{32}$$

294 For *Case A*, T_{max} in Eq. (27) equals to T_{pre}, and superscript A in above equations

295 refers to *Case A*.

296 Combining Eq. (25) and Eq. (32) gives the real force on the tunnel surface for *Case A*

297 (or for the pre-tensioned force)

298
$$T_{s}{}^{A} = \frac{K_{s}\left(K_{free} + K_{anch}\right)}{K_{s}K_{free} + K_{s}K_{anch} + K_{free}K_{anch}} T_{pre} \tag{33}$$

299 and from Eq. (24)

300
$$T_{rein}{}^{A} = \eta.T_{pre} \tag{34}$$

301
$$\eta = \frac{K_{free}K_{anch}}{K_{s}K_{free} + K_{s}K_{anch} + K_{free}K_{anch}} \tag{35}$$

14

302   Now, from Eq. (24), distribution of force can be obtained. As the initial anchored

303   length is assumed to be located beyond the plastic zone, the distribution of force in

304   that length of bolt is not here studied.

305   For *Case B*, the bolt is tensioned by both the pre-tensioned force (Fig. 4a) and the

306   movement of rock mass towards tunnel (Fig. 4b). The real force applied on the tunnel

307   surface by the pre-tensioned force can be calculated by a similar formulation of *Case*

308   *A*. The real force applied on the tunnel surface by the movement of rock mass can be

309   obtained by

310
$$T_s^{(2)} = \frac{K_s}{K_s + K_{rein}^{(2)}} T_{max}^{(2)} \tag{36}$$

311   where $K_{rein}^{(2)}$ is the axial stiffness of free length of the bolt where it is grouted after

312   pre-tensioning calculated by

313
$$K_{rein}^{(2)} = \frac{H}{\lambda} \left(\frac{e^{\lambda L} + e^{-\lambda L}}{e^{\lambda L} - e^{-\lambda L}} \right) \tag{37}$$

314   where L is the length of the bolt located in the plastic zone, and $T_{max}^{(2)}$ is the

315   maximum force of the bolt in the second step. It can be obtained by subtracting the

316   pre-tensioned force from the total maximum force in the ideal condition. (Superscripts

317   (1) and (2) refer to the first and second steps of the bolt tensioning, respectively).

318   The total real force on tunnel surface may be computed by

319
$$T_s^{(1)} + T_s^{(2)} = \frac{K_s \left(K_{free} + K_{anch} \right)}{K_s K_{free} + K_s K_{anch} + K_{free} K_{anch}} T_{pre} + \frac{K_s}{K_s + K_{rein}^{(2)}} T_{max}^{(2)} \tag{38}$$

320   Considering that Eq. (33) is the extension of Eq. (25), Eq. (38) will be

321
$$T_s^B = \frac{K_s}{K_s + K_{rein}^{(1)}} T_{pre} + \frac{K_s}{K_s + K_{rein}^{(2)}} \left(T_{max} - T_{pre} \right) \tag{39}$$

322   where T_s^B is the real force on the tunnel surface for *Case B*.

15

323   The distribution of real force along the bolt for *Case B* will be obtained by

324   •   For the first step (similar to *Case A*)

325
$$T^{(1)} = T_{pre} - T_{rein}^{(1)} \qquad\qquad 0 \le x < L_{free}$$

326   (40a)

327   •   For the second step (coupling behavior of the bolt and the rock mass)

328
$$T^{(2)} = T_{ideal}^{(2)} - \left[-\left(T_{max}^{(2)} - T_s^{(2)} \right) \frac{e^{-\lambda L}}{e^{-\lambda L} + e^{\lambda L}} e^{\lambda . x} - \left(T_{max}^{(2)} - T_s^{(2)} \right) \frac{e^{\lambda L}}{e^{-\lambda L} + e^{\lambda L}} e^{-\lambda . x} \right]$$

329
$$0 \le x < L_{free}$$

330   (40b)

331   where x denotes the arbitrary section of bolt length i.e. $x = 0$ at $r = r_i$ and $x = L$ at

332      $r = r_e$.

333   Therefore, summing of Equations (40a) and (40b), and after some manipulations, the

334   distribution of axial force along the bolt for *Case B* can be calculated as

335
$$T = T_{ideal} - \eta . T_{pre} - \left[-\left(T_{max} - T_{pre} \right)\left(1 - \beta \right)\left(\frac{e^{-\lambda L}}{e^{-\lambda L} + e^{\lambda L}} \right)\left(e^{\lambda . x} + e^{2\lambda L} e^{-\lambda x} \right) \right]$$

336   (41)

337   in which

338
$$\beta = \frac{K_s}{K_s + K_{rein}^{(2)}} \qquad\qquad (42)$$

339

340   **Calculation of tunnel convergence considering the real force**

341   As the obtained equilibrium equation is solved by the finite difference method (i.e.

342   Eq. (10)), Eq. (41) should be written as the iterative way. For ring $r_{(j)}$

16

343

$$T_{(j)} = T_{ideal(j)} - \eta . T_{pre} - \left[-\left(T_{max} - T_{pre} \right)\left(1 - \beta\right)\left(\frac{e^{-\lambda L}}{e^{-\lambda L} + e^{\lambda L}} \right)\left(e^{\lambda.(r_{(j)} - r_i)} + e^{2\lambda L}e^{-\lambda(r_{(j)} - r_i)} \right) \right]$$

344 (43)

345 Substituting Eq. (43) into Eq. (10) gives

346

$$\frac{\sigma_{r(j-1)} - \sigma_{r(j)}}{r_{(j-1)} - r_{(j)}} = \frac{\left[\frac{m_a \sigma_c}{2}\left(\sigma_{r(j)} + \sigma_{r(j-1)}\right) + s_a \sigma_c^2 \right]^{1/2}}{\frac{r_{(j)} + r_{(j-1)}}{2}} + \left| \frac{T_{(j-1)} - T_{(j)}}{r_{(j-1)} - r_{(j)}} . \frac{r_i}{C_0} . \frac{2}{r_{(j)} + r_{(j-1)}} \right|$$

347 (44)

348 The value of $T_{(j-1)} - T_{(j)}$ in the either side of neutral point (the location of maximum

349 force along the bolt) is the opposite to each other; the absolute value is used in Eq.

350 (44)

351 The similar performing process and defined parameters which were used to solve Eq.

352 (10) are applied to Eq. (44) except that the parameter $K_1 - \overline{K}_1$ (or $K_1 - K_1^e$) is

353 replaced by Eq. (45).

354

$$K_1 = \frac{T_{(j-1)} - T_{(j)}}{r_{(j-1)} - r_{(j)}} \frac{r_i}{C_0}$$

(45)

355 Hence, multipliers of the second order Eq. (13) will change to

356

$$b = \frac{K_1}{K} - \frac{\sigma_{r(j-1)}}{2K^2} - 2K_2 \qquad\qquad a = \frac{1}{4K^2}$$

357

$$c = \sigma_{r(j-1)}\left[\frac{\sigma_{r(j-1)}}{4K^2} - \frac{K_1}{K} - 2K_2 \right] + K_1^2 - s_a \sigma_c^2$$

358 (46)

359 Appendix B sets out the stepwise sequence of calculations provided in the section 2.

360 The consideration of a relative shear displacement results in a rotation of principal

361 stresses. That is, the radial and tangential stresses will not be longer principal stresses

362   as assumed in the ideal derivation of bolt force. However, it is assumed in this paper,

363   the produced shear stress is not so great that the principal stresses direction is greatly

364   changed to eclipse the results. It is a venial assumption at least in some conditions e.g.

365   where the pre-tensioned force value, the bolt's density, or rock mass Young's Modulus

366   is great.

367

368   **Examples**

369   A computer program was prepared to solve the differential equations developed by

370   the finite difference method.

371   **Example 1.** The proposed theoretical solution is applied to the Kielder experimental

372   tunnel to compare the accuracy of its results with the actual performance of bolts. The

373   Kielder Experimental Tunnel was driven through four rock mass types. The tunnel in

374   the mudstone was highly unstable, and required most support. The engineering

375   properties of mudstone are available in Table (1). Eight sections with different

376   support systems were constructed in which extensometers were also installed to

377   monitor movement of the rock mass. One of the sections was left unsupported while

378   two sections included combination of the passive grouted rockbolts and shotcrete.

379   One of the sections is also supported by passive grouted rockbolts only. The

380   geometrical parameters of two systems are available in Table (2).

381   According to Ward et al. (1976), total short-term movement of tunnel surface in the

382   unsupported section of mudstone was about 8 *mm* in which less than1 *mm* had

383   occurred before the face reached, and about 6 *mm* when the face had advanced 2 *m*

384   beyond this position. If the reinforcement system was installed just in front of the

18

385   face, it can be expected that tunnel closure was about 1-2 *mm* prior to bolt installation

386   (assumed value is 1.5 *mm* in this paper).

387   Fig. (5) shows the corresponding ground response curves, and Table (3) gives the

388   calculated and the measured deformations data at tunnel surface for the supported

389   and unsupported rock mass (sequence of calculations was performed by the algorithm

390   presented in Appendix B). As observed, the proposed method can almost predict the

391   identical results and agree with the in-situ measurements in a satisfactory way.

392   A perfect constraint from the end- plate is predicted in the case of using rockbolt

393   together with shotcrete. This is because, a complete planner contact between the bolt

394   head and the tunnel surface is obtained, and the bolts will take higher loads at the

395   tunnel surface in comparison with the condition that not perfect constraint is foreseen.

396   **Example 2.** A highway tunnel with 10.7 *m* in diameter is driven in a fair to good

397   quality limestone at a depth of 122 *m* below the surface (Brown et al. 1983). The

398   material property data for the rock mass and in-situ stress are available in Brown et al.

399   (1983).

400   The pre-tensioned grouted rockbolts are installed by $T_{pre-ten} = 17$ *ton* with $C_0 = 1$ m^2,

401    $L = 3.15$ *m* when the fictitious constrained pressure is $p_{inst} = 16.5$ ton/m^2 (the

402   other parameters is assumed to be similar to Example 1). If it is assumed a complete

403   constrained is provided by the end plate, the pre-tensioned pressure is greater than the

404   fictitious constrained pressure of tunnel face. Consequently, the circumstance of *Case*

405   *A* will take place. The output results are shown in Fig. (6) and Table (4). The

406   efficiency of pre-tensioning can now be best assessed and observed. Therefore, the

407   convergence of tunnel by the pre-tensioning of bolts is reduced considerably.

19

408   If the pre-tensioned grouted rockbolts are installed by $T_{pre-ten} = 10 \quad ton$, the

409   circumstance of *Case B* will take place. Fig. (6) shows the ground response curve for

410   this case.

411

412   **A new practical method for the design of the pre-tensioned**

413   **grouted bolts**

414   Although the proposed model almost predicts the accurate performance of the passive

415   and the pre-tensioned grouted bolts, its formulas are too complicated to be used as a

416   preliminary design tool, and always need a computer program to carry out the

417   computation procedures. Hence, it will be worth introducing a simple method on the

418   basis of new presented approach parameters to be used as a rule of thumb method in

419   practice.

420   For *Case A*, the bolt and the rock mass interaction behavior is similar to that of the

421   support systems (such as shotcrete or the pre-tensioned un-grouted bolts) rather than

422   to the reinforcement systems. Therefore, Ground Response Curve (GRC) of the un-

423   supported rock mass and Support Characteristic Curve of a pre-tensioned bolt are

424   plotted (solid line for this Case) to obtain the ultimate tunnel convergence. As seen in

425   Fig. (7), the ultimate convergence is equal to that in the installation time.

426   The pre-tensioned un-grouted bolt characteristic curve can be obtained by the Eq. (47)

427   (Stille et al. 1989)

428
$$p_i = k_{sys}.\Delta u_i + p_{pre-ten} \tag{47}$$

429   where k_{sys} is the support system stiffness calculated by (Stille et al. 1989)

430
$$k_{sys} = \frac{A_b.E_b}{C_0} \frac{1}{L_{free}} \frac{1}{\xi} \tag{48}$$

431 Eq. (48) is the stiffness of support system which the reinforcement effect is smeared

432 within the zone of its influence. Thus, the stiffness of a single element is calculated by

433
$$k = \frac{A_b.E_b}{L_{free}} \frac{1}{\xi} = K_{free} \frac{1}{\xi}$$

434 (49)

435 ξ is a factor describing the local deformations occurring in the anchoring zone (the

436 far boundary), under the end plate and the bolt head (the near boundary). Stille et al.

437 (1989) pointed out that ξ is an empirical factor which can be determined from Hoek

438 and Brown's (1980) published pull-out tests data of a variety of mechanical and

439 chemically anchored rockbolts. However, those data were not guaranteed to give the

440 accurate results, and were strongly recommended to be determined from field tests on

441 the bolts for critical applications.

442 It seems that it will be worth developing an analytical approach to obtain ξ.

443 Flexibility of the complex of bolt head component and the initial anchored length lead

444 to decreasing the axial stiffness of single reinforcement. This is because their

445 deformations under the applied force reduce bolt elongation.

446 On the other hand, according to the proposed method, the axial stiffness of pre-

447 tensioned un-grouted rockbolt can be calculated by

448
$$\frac{1}{K_b} = \frac{1}{K_{anch}} + \frac{1}{K_{free}} + \frac{1}{K_s}$$
(50)

449 where K_b is total axial stiffness of reinforcement element.

450 Equating right hand of Eq. (50) with that of Eq. (49), and then simplifying gives

451
$$\xi = 1 + \frac{K_{free}}{K_{anch}} + \frac{K_{free}}{K_s}$$
(51)

452   For *Case B*, the ultimate tunnel convergence will be at the intersection point of the

453   diagonal line of Support characteristic curve and the Ground Response Curve of the

454   un-supported rock mass (Dashed line in Fig. 7).

455   However, this solution is not very exact in case the entire length of the bolt is grouted,

456   and the bolt interacts with its surrounding grout and rock mass. In other words, the

457   bolts confine tunnel convergence not only by applying radial pressure to tunnel

458   surface (like the support systems e.g. un-grouted pre-tensioned bolts), but also by

459   improving rock mass strength quality (like the reinforcement systems e.g. the passive

460   grouted rockbolts).

461   Therefore, to extend this new approach for *Case B*, the pre-tensioned grouted

462   rockbolts behavior is simulated as a combination of both the support and the

463   reinforcement systems. That is, the improved rock mass and the pre-tensioned un-

464   grouted bolts act independently. The ground response curve of reinforced rock mass

465   by the passive grouted rockbolts is calculated and plotted, and then the support

466   characteristic curve of the pre-tensioned un-grouted bolts plotted separately. The

467   intersection point of two curves gives tunnel convergence which is reinforced by pre-

468   tensioned grouted rockbolts.

469   No end-plate should be considered for the passive grouted rockbolts. This is because

470   the end-plate effect is taken into account in the behavior of un-grouted pre-tensioned

471   bolt. If the end-plate does not exist, then K_s will be zero, and $T_s = 0$. Consequently

472   the distribution of axial stress along the passive grouted bolts without the end-plate is

$$T^{pass} = T_{ideal}{}^{pass} - \left[-T_{\max}{}^{pass} \frac{e^{-\lambda L}}{e^{-\lambda L} + e^{\lambda L}} e^{\lambda.x} - T_{\max}{}^{pass} \frac{e^{\lambda L}}{e^{-\lambda L} + e^{\lambda L}} e^{-\lambda.x} \right]$$

473

474   (52)

475   Superscript *pass* refers to the passive grouted bolts.

476   This new approach is employed to solve Example 2 for *Case B*. The output results are

477   available in Table (5) and Fig. (8). The intersection point of the support characteristic

478   curve and the ground response curve of the reinforced tunnel (by the passive grouted

479   bolts without face-plate) gives the ultimate convergence of tunnel. As observed, this

480   approach predicts almost the identical convergence obtained in Example 2.

481   The convergence of tunnel supported by un-grouted pre-tensioned rockbolts is almost

482   identical to that of employing the grouted types. In other words, the grouting effect of

483   bolt is not very effective, and can be neglected. However, on the basis of the proposed

484   model concepts and as it can be seen from Fig. (8), when either the pre-tensioned

485   force is not great enough or the stiffness of the pre-tensioned bolt system is small (e.g.

486   the value of ξ is great), the grouting effect can be considerable.

487   As a practical design tool, if complete constraint is provided for the near end of bolt

488   head, the pre-tensioned fully grouted bolts can be treated as un-grouted types and its

489   grouting effect is only considered as a factor improving safety.

490

491   **Conclusions**

492   New analytical approach was proposed for the design the pre-tensioned grouted

493   rockbolts in tunnels based on convergence confinement method. The relationship

494   between the value of constrained radial stress at bolt installation time and the value of

495   applied pre-tensioned pressure was focused on in process of modeling. The near and

496   far boundaries conditions of bolt were also analytically modeled because they can

497   affect the performance of pre-tensioned bolts.

498 Due to the complexity of theoretical approach for design purposes, a simple method

499 on the basis of new given approach was finally introduced.

500 The practical outcome of this paper is that if the complete constraint is provided for

501 the near end of bolt head, the grouting effect of the pre-tensioned fully grouted bolts

502 on tunnel stability can be neglected. Therefore, they can be designed by the similar

503 approach of un-grouted pre-tensioned bolts. However, if it is not possible to apply

504 sufficient pre-tensioned force to the bolts (the pre-tensioned force is not great

505 enough), if the anchoring system of bolt is not proper e.g. using the expansion shell or

506 weak grout, or if the complete planner contact between the bolt head and the tunnel

507 surface is not predicted, the grouting effect will be considerable and the attention

508 should be taken to grout quality.

509

510 **Appendix A.**

511 **(I) Calculation of the axial stiffness of anchored length and full length of grouted**

512 **rockbolt**

513 As the pre-tensioned force is applied, the free and the anchored length of the bolt are

514 tensioned. The equilibrium of the axial force in the anchored length is

515 $$T + dT = T + \tau.\pi.d_b.dx \qquad (53)$$

516 where T is the force in the anchored length, d_b is diameter of bolt, and τ is the shear

517 stress on reinforcement perimeter which can be obtained by

518 $$\tau = K_{ini}.v \qquad (54)$$

519 where v is the relative displacement between the rock mass and the bolt, K_{ini} is the

520 initial shear stiffness between the bolt and the rock mass expressed as (Cai et al.

521 2004a,b)

$$K_{ini} = \frac{H}{\pi d_{rein}} \tag{55}$$

522

523 where H is a material parameter associated to the shear stiffness between the bolt and

524 the rock mass and can be computed by Eq. (56)

$$H = \frac{2\pi G_g G_m}{[\ln(R/r_b) - 1/2]G_g + \ln(r_g/r_b)G_m} \tag{56}$$

525

526 where r_b and r_g are radius of the bolt and radius of the grout borehole; G_g and G_m is

527 shear modulus of the grout mortar and the rock mass, respectively; and R is the

528 influence radius of a single rock bolt.

529 Substituting Eq. (54) into Eq. (53) and then taking derivation gives

$$\frac{d^2 T}{dx^2} - \lambda^2 T = 0 \tag{57}$$

530

531 in which

$$\frac{dv}{dx} = \frac{T}{E_b . A_b} \tag{58}$$

532

$$\lambda = \left(\frac{K_{ini} . \pi d_b}{E_b A_b}\right)^{0.5} = \left(\frac{H}{E_b A_b}\right)^{0.5} \tag{59}$$

533

534 A_b and E_b are the area section and the elastic modulus of the bolt, respectively.

535 The solution of above differential equation is

$$T = C_1 e^{\lambda . x} + C_2 e^{-\lambda . x} \tag{60}$$

536

537 C_1 and C_2 are constants obtained by the following boundary conditions

538 At $\quad\quad\quad x = L_{free} \quad\quad\quad T = -T_{rein} = -(T_{max} - T_s)$

539 and $\quad\quad$ at $\quad\quad x = L_{free} + L_{anch} \quad\quad v = 0$

25

540   where L_{free} is the free length of the bolt which is not grouted in pre-loading process,

541   L_{anch} is the initially anchored length of the bolt securing the anchoring capacity

542   against pre-loading.

543   Note that T_{max} is equal to T_{pre} for *Case A*, (and also for the first step of *Case B*).

544   Because, the maximum force is T_{pre} for this case.

545   Substituting C_1 and C_2 into Eq. (60) and then calculating v at $x = L_{free}$ gives the

546   magnitude of displacement of the bolt in anchored section i.e.

547
$$v_{anch} = \frac{\lambda . T_{rein}}{H} \left(\frac{e^{\lambda L_{anch}} - e^{-\lambda L_{anch}}}{e^{\lambda L_{anch}} + e^{-\lambda L_{anch}}} \right) \tag{61}$$

548   therefore

549
$$K_{anch} = \frac{H}{\lambda} \left(\frac{e^{\lambda L_{anch}} + e^{-\lambda L_{anch}}}{e^{\lambda L_{anch}} - e^{-\lambda L_{anch}}} \right) \tag{62}$$

550   K_{anch} is the axial stiffness of bolt in the anchored section.

551   Performing the same process for the second step of *Case B* with the following

552   boundary condition

553   At $x = 0$ $T = -T_{rein}^{(2)} = -\left(T_{max} - T_{pre} \right) - T_s^{(2)}$

554   and at $x = L$ $v = 0$

555   gives

556
$$K_{rein}^{(2)} = \frac{H}{\lambda} \left(\frac{e^{\lambda L} + e^{-\lambda L}}{e^{\lambda L} - e^{-\lambda L}} \right) \tag{63}$$

557   where T_{max} is the force on the bolt head in the ideal connection between the bolt and

558   the rock mass, and $T_s^{(2)}$ is the force on the bolt head applied on the tunnel surface in

559 real condition. Superscript (2) refers to the second step of the bolt tensioning which

560 is due to rock mass movement towards tunnel.

561

562 **(II) Estimation of K_s**

563 From the analysis of the in situ measurements and the results of numerous bi-

564 dimensional numerical calculation in the performed parametric study, Oreste (2008)

565 presented the axial force along the passive grouted bolts, with a certain

566 approximation, by a simple two-line graphic (Fig. 9). When a perfect constraint on the

567 bolt head is predicted, the maximum value of bolt force is at the distance of about

568 $L/6$ from the tunnel wall while the value in the bolt head (T_s) is $2/3$ of the

569 maximum force along the bolt i.e.

$$T_s = \frac{2}{3}T'_{\max} \qquad (64)$$

570

571 As the distribution of axial force in the "pick up length" is exponential, it can be

572 written $T_s = (0.35 - 0.5)T_{\max}$ (Ranjbarnia 2014). Therefore

$$K_s = (0.5 - 0.8)K_{rein} \qquad (65)$$

573

574 Evaluation of the results of theoretical approaches carried out for the modelling of

575 passive grouted bolts (Stille et al. 1989; Oreste and Peila 1996; Li and Stillborg 1999,

576 Cai et al. 2004a) and in-situ measurements (Ward et al. 1976) shows the suitability of

577 Eq. (65).

578 K_{rein} in Eq. (65) is obtained by Eq. (42). This is because; it gives the reinforcement

579 stiffness for the second step of loading which is identical to the loading process of the

580 passive grouted bolts.

581

582 **Appendix B. Ground response curve calculation for reinforced**

583 **tunnel**

584 *Input data.*

585 σ_c : un- axial compressive strength of intact rock pieces.

586 m , s : material constants for original rock mass.

587 E_m , v : Young's modulus and Poisson's ratio of original rock mass.

588 G_g : shear modulus grout.

589 m_r , s_r : material constants for broken rock mass.

590 f , h : gradients of $-\varepsilon_3^p$ vs. ε_1^p lines in the residual and the strain softening stages,

591 respectively.

592 μ : constant defining strain at which residual strength is reached.

593 p_0 : in situ hydrostatic stress.

594 r_i : tunnel radius.

595 d_b : the bolt diameter.

596 d_g : the hole diameter.

597 A_b : cross section area of each bolt.

598 E_s : Young's modulus of bolt.

599 C_0 : bolt's spacing.

600 $T_{pre-ten}$: pre-tensioning force.

601 L_{anch} : initial anchored length.

602 L : total bolt length.

603 R : the influence limit of each bolt usually is $10d_g$

28

604

Preliminary Calculations

606   1) $M = \dfrac{1}{2}\left[\left(\dfrac{m}{4}\right)^2 + m\dfrac{p_0}{\sigma_c} + s\right]^{1/2} - \dfrac{m}{8}$

607   2) $G_m = \dfrac{E_m}{2(1+\upsilon)}$

608   3) $H = \dfrac{2\pi G_g G_m}{\left[\ln(R/r_b) - 1/2\right]G_g + \ln(r_g/r_b)G_m}$

609   4) $\lambda = \left(\dfrac{H}{E_s . A_b}\right)^{0.5}$

610   5) $p_{pre-ten} = T_{pre-ten}/(C_0)$

611   6) $\varepsilon_{pre-ten} = T_{pre-ten}/(A_b . E_s)$

612   7) $L_{free} = L - L_{anch}$

613   8) $K_{rein} = \dfrac{H}{\lambda}\left(\dfrac{e^{\lambda L} + e^{-\lambda L}}{e^{\lambda L} - e^{-\lambda L}}\right)$

614   9) $K_s = \chi . K_{rein}$ $0.5 < \chi < 0.8$

615   10) $K_{anch} = \dfrac{H}{\lambda}\left(\dfrac{e^{\lambda L_{anch}} + e^{-\lambda L_{anch}}}{e^{\lambda L_{anch}} - e^{-\lambda L_{anch}}}\right)$

616   11) $K_{free} = \dfrac{E_b . A_b}{L_{free}}$

617   12) $K_{rein}{}^{(1)} = \dfrac{K_{free} . K_{anch}}{K_{free} + K_{anch}}$

618   13) $K_{rein}{}^{(2)} = \dfrac{H}{\lambda}\left(\dfrac{e^{\lambda L} + e^{-\lambda L}}{e^{\lambda L} - e^{-\lambda L}}\right)$

619   14) $\alpha = \dfrac{K_s}{K_s + K_{rein}^{(1)}}$

620   15) $\beta = \dfrac{K_s}{K_s + K_{rein}^{(2)}}$

621   16) $\eta = \dfrac{K_{free} K_{anch}}{K_s K_{free} + K_s K_{anch} + K_{free} K_{anch}}$

622

Calculations for the first ring

624   1) $r_{(1)} = r_e$

625   2) $\varepsilon_{\theta(1)} = \varepsilon_{\theta(e)} = M\sigma_c / 2G$

626   3) $\varepsilon_{r(1)} = \varepsilon_{r(e)} = -M\sigma_c / 2G$

627   4) $\sigma_{r(1)} = \sigma_{re} = p_0 - M.\sigma_c$

628   5) $\sigma_{\theta(1)} = \sigma_{\theta e} = p_0 + M.\sigma_c$

629   6) $m_{(1)} = m$

630   7) $s_{(1)} = s$

631   8) $\omega_{(1)} = 0$

632   9) $\zeta_1 = r_{(1)} / r_e = 1$

633

Sequence of calculations for each ring

635   1) $d\varepsilon_\theta = 0.005\varepsilon_{\theta(1)}$

636   2) $\varepsilon_{\theta(j)} = \varepsilon_{\theta(j-1)} + d\varepsilon_\theta$

637   3) If $\varepsilon_{\theta(j)} \le \mu.\varepsilon_{\theta(1)}$ then $\varepsilon_{r(j)} = \varepsilon_{r(j-1)} - hd\varepsilon_\theta$ otherwise $\varepsilon_{r(j)} = \varepsilon_{r(j-1)} - fd\varepsilon_\theta$

638   4) $\kappa = \dfrac{2\varepsilon_{\theta(j-1)} - \varepsilon_{r(j-1)} - \varepsilon_{r(j)}}{2\varepsilon_{\theta(j)} - \varepsilon_{r(j-1)} - \varepsilon_{r(j)}}$

639   5) $\zeta_{(j)} = \kappa.\zeta_{(j-1)}$

640   6) $\lambda_{(j)} = r_{(j)} / r_e \quad \lambda_{(j-1)} = r_{(j-1)} / r_e$

641   7) If $\varepsilon_{\theta(j)} \le \mu\varepsilon_{\theta(1)}$ then $m_{(j)} = m + (m_r - m)\dfrac{\varepsilon_{\theta(j)} - \varepsilon_{\theta(e)}}{(\mu-1)\varepsilon_{\theta(e)}}$ otherwise $m_{(j)} = m_r$

642   8) If $\varepsilon_{\theta(j)} \le \mu\varepsilon_{\theta(1)}$ then $s_{(j)} = s + (s_r - s)\dfrac{\varepsilon_{\theta(j)} - \varepsilon_{\theta(e)}}{(\mu-1)\varepsilon_{\theta(e)}}$ otherwise $s_{(j)} = s_r$

643   9) $m_a = \dfrac{1}{2}\left(m_{(j-1)} + m_{(j)}\right)$

644   10) $s_a = \dfrac{1}{2}\left(s_{(j-1)} + s_{(j)}\right)$

645   11) $K_2 = \dfrac{m_a\sigma_c}{4}$

646   12) $K = \dfrac{\lambda_{(j-1)} - \lambda_{(j)}}{\lambda_{(j)} + \lambda_{(j-1)}}$

647   13) If $p_{pre-ten} \ge p_{inst}$, then go to step 14, otherwise go to step 18

648   14) $a = \dfrac{1}{4K^2}$

649   15) $b = -\dfrac{\sigma_{r(j-1)}}{2K^2} - 2K_2$

650   16) $c = \sigma_{r(j-1)}\left[\dfrac{\sigma_{r(j-1)}}{4K^2} - 2K_2\right] - s_a\sigma_c^2$

651   17) Now, go to step 26

652   18) If $\sigma_{r(j-1)} > p_{inst}$ and then $\omega_{(j)} = 0$, other wise $\omega_{(j)} = \omega_{(j-1)} + 1$

653   19) $\gamma = d\varepsilon_{r(j)} = \varepsilon_{r(j)} - \varepsilon_{r(j-1)}$

31

654   20) $K_1 = \dfrac{A_b E_s r_i}{C_0 \left(r_{(j-1)} - r_{(j)}\right)} \gamma$

655   21) $\bar{\gamma} = d\bar{\varepsilon}_{r(j)} = \bar{\varepsilon}_{r(j-\omega_j)} - \bar{\varepsilon}_{r(j-1-\omega_j)}$ $r_i \leq r < \bar{r}_e$

656    $\gamma^e = d\varepsilon^e_{r(j)} = \varepsilon^e_{r(j)} - \varepsilon^e_{r(j-1)}$ $\bar{r}_e \leq r \leq r_e$

657   22) $\bar{K}_1 = \dfrac{A_b E_s r_i}{C_0 \left(r_{(j-1)} - r_{(j)}\right)} \bar{\gamma} \ \ r_i \leq r < \bar{r}_e$

658    $\bar{r}_e \leq r \leq r_e$ $K_1^e = \dfrac{A_b E_s r_i}{C_0 \left(r_{(j-1)} - r_{(j)}\right)} \gamma^e$

659   23) $a = \dfrac{1}{4K^2}$

660   24) $b = -\dfrac{K_1 - \bar{K}_1}{K} - \dfrac{\sigma_{r(j-1)}}{2K^2} - 2K_2 \ \ r_i \leq r < \bar{r}_e$

661    $\bar{r}_e \leq r \leq r_e$ $b = -\dfrac{K_1 - K_1^e}{K} - \dfrac{\sigma_{r(j-1)}}{2K^2} - 2K_2$

662   25) $c = \sigma_{r(j-1)} \left[\dfrac{\sigma_{r(j-1)}}{4K^2} + \dfrac{K_1 - \bar{K}_1}{K} - 2K_2 \right] + \left(K_1 - \bar{K}_1\right)^2 - s_a \sigma_c^2$

663    $r_i \leq r < \bar{r}_e$

664    $c = \sigma_{r(j-1)} \left[\dfrac{\sigma_{r(j-1)}}{4K^2} + \dfrac{K_1 - K_1^e}{K} - 2K_2 \right] + \left(K_1 - K_1^e\right)^2 - s_a \sigma_c^2$

665    $\bar{r}_e \leq r \leq r_e$

666   26) $\Delta = b^2 - 4a.c$

667   27) $\sigma_{r(j)} = \dfrac{-b - \sqrt{\Delta}}{2a}$

668   28) If $\sigma_{r(j)} > p_i$, then increment j by 1 and repeat the calculation sequence for next

669   ring.

670   29) If $\sigma_{r(j)} \approx p_i$, then $r_{(j)} = r_i$; $r_e = r_{(j)} / \lambda_{(j)}$.

32

671 Note: p_i should not be decreased from $p_{pre-ten}$.

672 30) If $\sigma_{r(j)} \approx p_{inst}$, then $\bar{r}_e = r_e$

673 31) The radii of all the rings may now be calculated, using $r_{(j)} = \lambda_{(j)}.r_e$

674 32) The displacement values of rings may be determined from the previously

675 computed values of $u_j = -\varepsilon_{\theta(j)}.r_{(j)}$

676 33) $T_{ideal(j)} = A_b.E_s.\left(\varepsilon_{r(j)} - \varepsilon_{r(j-\omega_j)} + \varepsilon_{pre-ten}\right)$

677 34) If $\sigma_{r(j)} \approx \min\{p_{inst}, p_{pre-ten}\}$, then $T_{ideal(j)} = T_{max}$

678 35) After calculating T_{max}, the steps 1 to 12 are repeated.

679 36) $T_s = (1-\eta)T_{pre}$

680 37) $p'_{pre-ten} = T_s/C_0$

681 38) If $p'_{pre-ten} \geq p_{inst}$, then $T_{(j)} = (1-\eta)T_{pre}$ and go to step 39, otherwise go to step 40

682 39) the steps 14 to 16 and steps 26 to 29 are repeated except that $p_{inst} < p_i < p_0$. Go to

683 step 46.

684 40) $T_{(j)} = T_{ideal(j)} - \eta.T_{pre} - \left[-\left(T_{max} - T_{pre}\right)(1-\beta)\left(\frac{e^{-\lambda L}}{e^{-\lambda L} + e^{\lambda L}}\right)\left(e^{\lambda.\left(r_{(j)}-r_i\right)} + e^{2\lambda L}e^{-\lambda\left(r_{(j)}-r_i\right)}\right)\right]$

685 41) $K_1 = \dfrac{T_{(j-1)} - T_{(j)}}{r_{(j-1)} - r_{(j)}} \dfrac{r_i}{C_0}$

686 42) $a = \dfrac{1}{4K^2}$

687 43) $b = \dfrac{K_1}{K} - \dfrac{\sigma_{r(j-1)}}{2K^2} - 2K_2$

688 44). $c = \sigma_{r(j-1)}\left[\dfrac{\sigma_{r(j-1)}}{4K^2} - \dfrac{K_1}{K} - 2K_2\right] + K_1^2 - s_a\sigma_c^2$

33

689   45) Steps 26 to 29 are repeated except that $p'_{pre-ten} < p_i < p_0$.

690   46) The radii of all the rings may now be calculated, using $r_{(j)} = \lambda_{(j)} \cdot r_e$

691   47) The displacement values of rings may be determined from the previously

692   computed values of $u_j = -\varepsilon_{\theta(j)} \cdot r_{(j)}$.

693

694   **References**

695   Aydan, Ö. (1989). "The Stabilisation of Rock Engineering Structures by Rockbolts."

696   Ph. D. thesis, Queens's Univ., Kingston, Ontario.

697

698   Bischoff, J.A., Smart, J.D. (1975). "A method of computing a rock reinforcement

699   system which is structurally equivalent to an internal support system." *Proc. of 16th*

700   *Symp. on Rock Mechanics,* Univ. of Minnesota, 179-184.

701

702   Bobet, A. (2006). "A simple method for analysis of point anchored rockbolts in

703   circular tunnels in elastic ground." *Rock Mech. Rock Eng.*, 39, 315- 338.

704

705   Bobet, A., Einstein, E. (2011). "Tunnel reinforcement with rockbolts." *Tunnel.*

706   *Underground Space Tech.,* 26, 100-123.

707

708   Brown, E.T., Bray, J.W., Ladanyi, B., and Hoek, E. (1983). "Ground response curves

709   for rock tunnels." *J. of Geotech. Eng.,* 109, 15- 39.

710

711 Cai, Y., Esaki, T., and Jiang, Y. (2004a). "An analytical model to predict axial load in

712 grouted rock bolt for soft rock tunneling." *Tunnel. Underground Space Tech.,* 19,

713 607- 618.

714

715 Cai, Y., Jiang, Y.J., and Esaki, T. (2004b). "A rock bolt and rock mass interaction

716 model." *Int. J. of Rock Mech. Mining Sci.,* 41, 1055-1067.

717

718 Carranza-Torres, C. (2009). "Analytical and Numerical Study of the Mechanics of

719 Rockbolt Reinforcement around Tunnels in Rock Masses." *Rock Mech. Rock Eng.*,

720 42, 175- 228.

721

722 Fahimifar, A., Soroush, H. (2005). "A theoretical approach for analysis of the

723 interaction between grouted rockbolts and rock masses." *Tunnel. Underground Space*

724 *Tech.,* 20, 333-343.

725

726 Fahimifar, A., Ranjbarnia, M. (2009). "Analytical approach for the design of active

727 grouted rockbolts in tunnel stability based on convergence-confinement method."

728 *Tunnel. Underground Space Tech.,* 24, 363-375.

729

730 Freeman, T.J. (1978). "The behavior of fully-bonded rock bolts in the Kielder

731 experimental tunnel." *Tunnels Tunn*, 37–40.

732

733 Grasso, P.G., Mahtab, A., and Pelizza, S. (1989). "Riqualificazione della massa

734 roccoisa: un criterio per la atabilizzaazione della gallerie." *Gallerie e Grandi Opere*

735 *Sotterranee*, 29, 35- 41.

736

737   Guan, Zh., Jiang, Y., Tanabasi, Y., and Huang, H. (2007). "Reinforcement mechanics

738   of passive bolts in conventional tunneling." *Int. J. of Rock Mech. Mining Sci.,* 44,

739   625-636.

740

741   Hoek, E., Brown, E.T. (1980). "Underground Excavations in Rock." The Institution

742   of Mining and Metallurgy, London.

743

744   Huang, Z., Broch, E., and Lu, M. (2002). "Cavern roof stability- mechanism of

745   arching and stabilization by rockbolting." *Tunnel. Underground Space Tech.,* 17, 249-

746   261.

747

748   Indraratna, B., Kaiser, P.K. (1990a). "Design of grouted rock bolts based on the

749   convergence control method." *Int. J. Rock Mech. Mining Sci and GeoMech.,* 27, 269-

750   281.

751

752   Indraratna, B., Kaiser, P.K. (1990b). "Analytical model for the design of grouted rock

753   bolts." *Int. J. Numer. Anal. Meth. Geomech.*, 14, 227- 251.

754

755   Li, C., Stillborg, B. (1999). "Analytical models for rock bolts." *Int. J. of Rock Mech.*

756   *Mining Sci.,* 36, 1013- 1029.

757

758   Oreste P.P., Peila, D. (1996). "Radial passive rockbolting in tunneling design with a

759   new convergence-confinement model." *Int. J. Rock Mech. Mining Sci and GeoMech.,*

760   33, 443- 454.

761

762   Osgoui, R.R., Oreste, P. (2010). "Elasto-plastic analytical model for the design of

763   grouted bolts in a Hoek–Brown medium." *Int. J. Numer. Anal. Meth. Geomech.*, 34,

764   1651–1686.

765

766   Oreste, P.P. (2008). "Distinct analysis of fully grouted bolts around a circular tunnel

767   considering the congruence of displacements between the bar and the rock." *Int. J. of*

768   *Rock Mech. Mining Sci.,* 45, 1052–1067.

769

770   Peila, D., Oreste P.P. (1995). "Axisymmetric analysis of ground reinforcing in

771   tunneling design." *Comput. Geomach.,* 17, 253- 274.

772

773   Ranjbarnia, M., (2014). "Theoretical analysis of pre-tensioned grouted rockbolts

774   behavior in tunnels considering the interaction of bolt, grout, and rock mass", *PhD*

775   *thesis*, Department Civil and Environmental Engineering, Amirkabir University of

776   Technology, Tehran. Iran

777

778   Stille, H., Holmberg, M., and Nord G. (1989). "Support of Weak Rock with Grouted

779   Bolts and Shotcrete." *Int. J. of Rock Mech. Mining Sci. and Geomech.* 26, 99-l 1
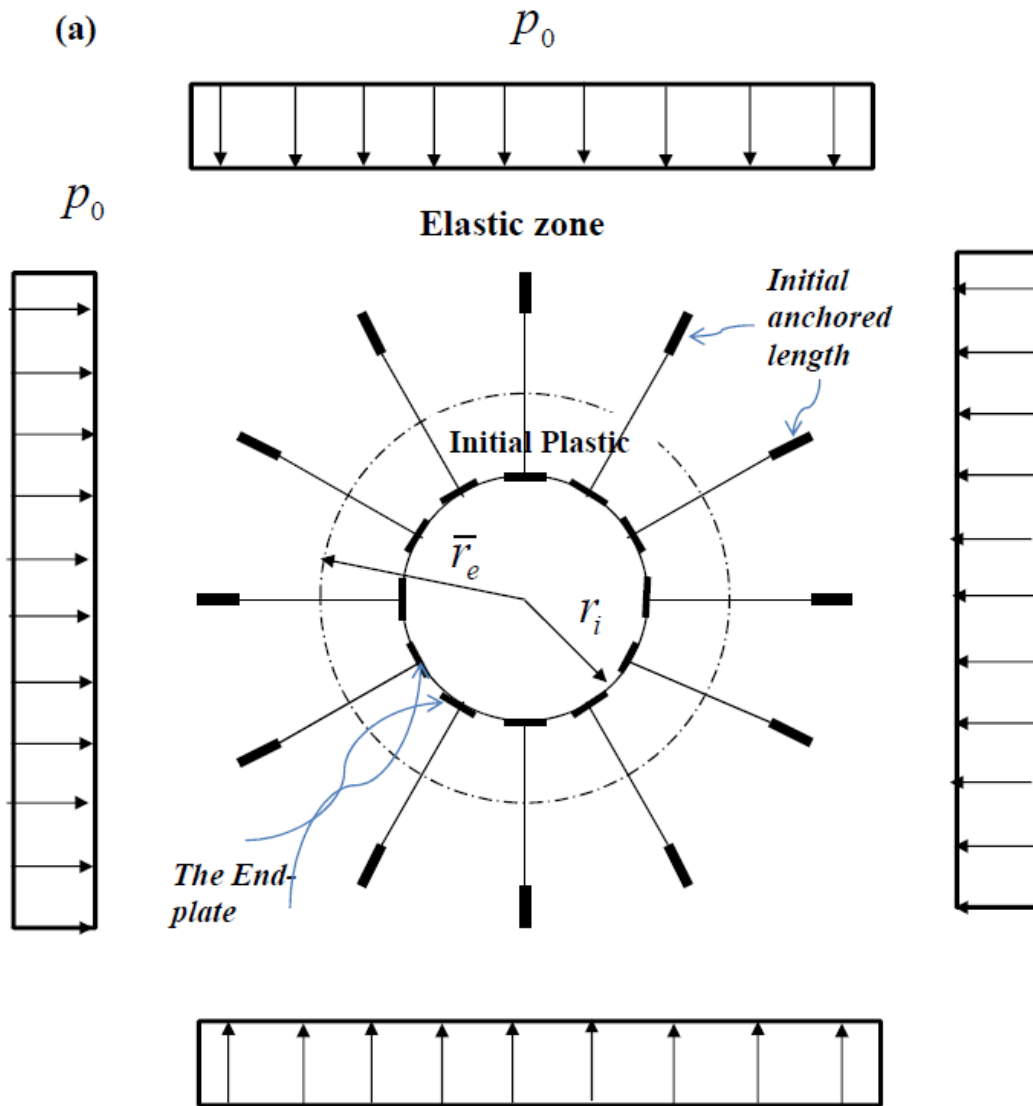
780

781   Ward, W.H., Coats, D.J., and Tedd, P. (1976). "Performance of support systems in the

782   Four Fathom Mudstone." *Proc. of Tunnelling 76*, London, 329-340.

783

784

785

787

788   Figure 1. Circular tunnel reinforced by systematic pre-tensioned grouted bolts (a) the

789   plastic radius at the bolt installation time (b) Increasing tunnel plastic radius
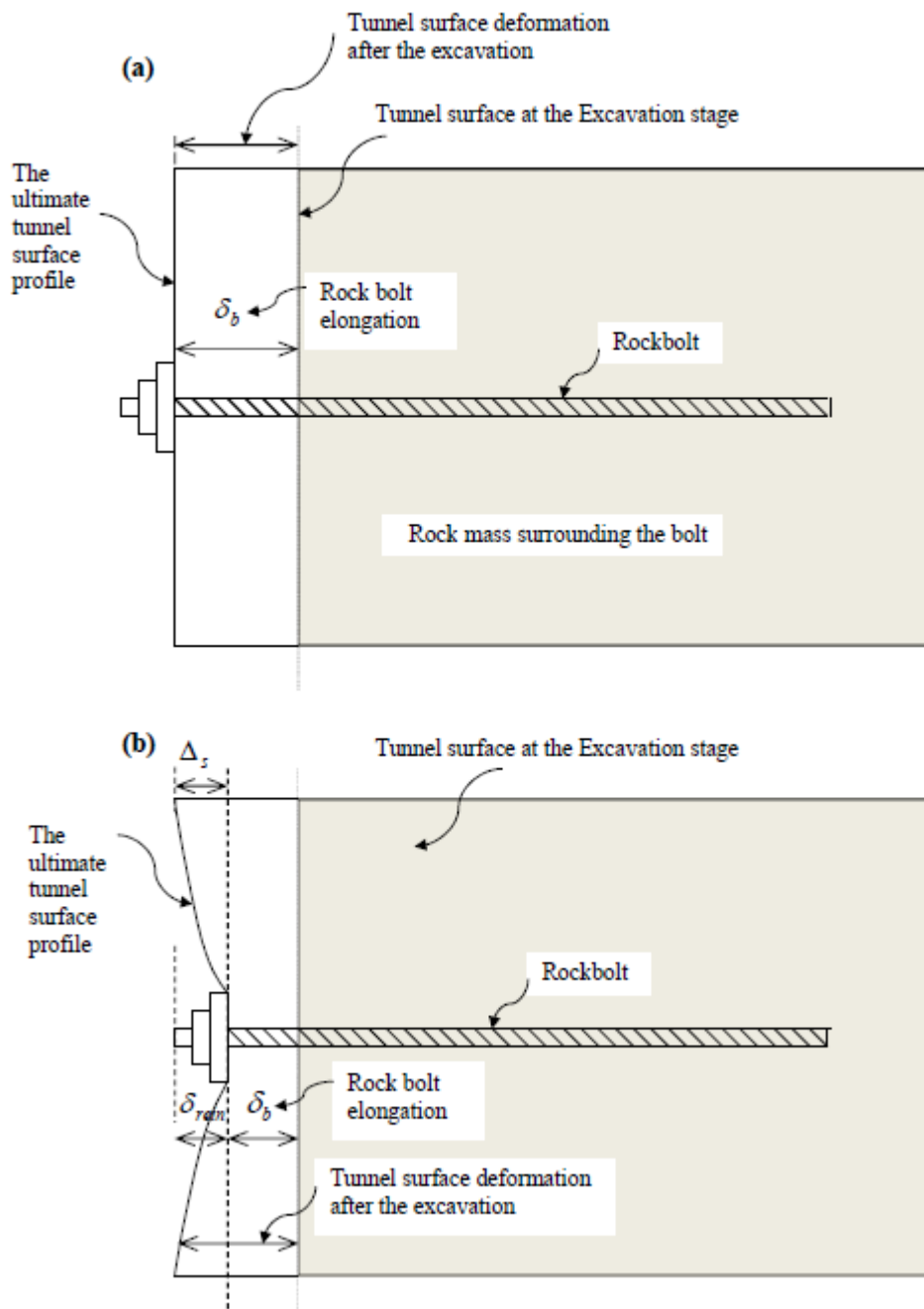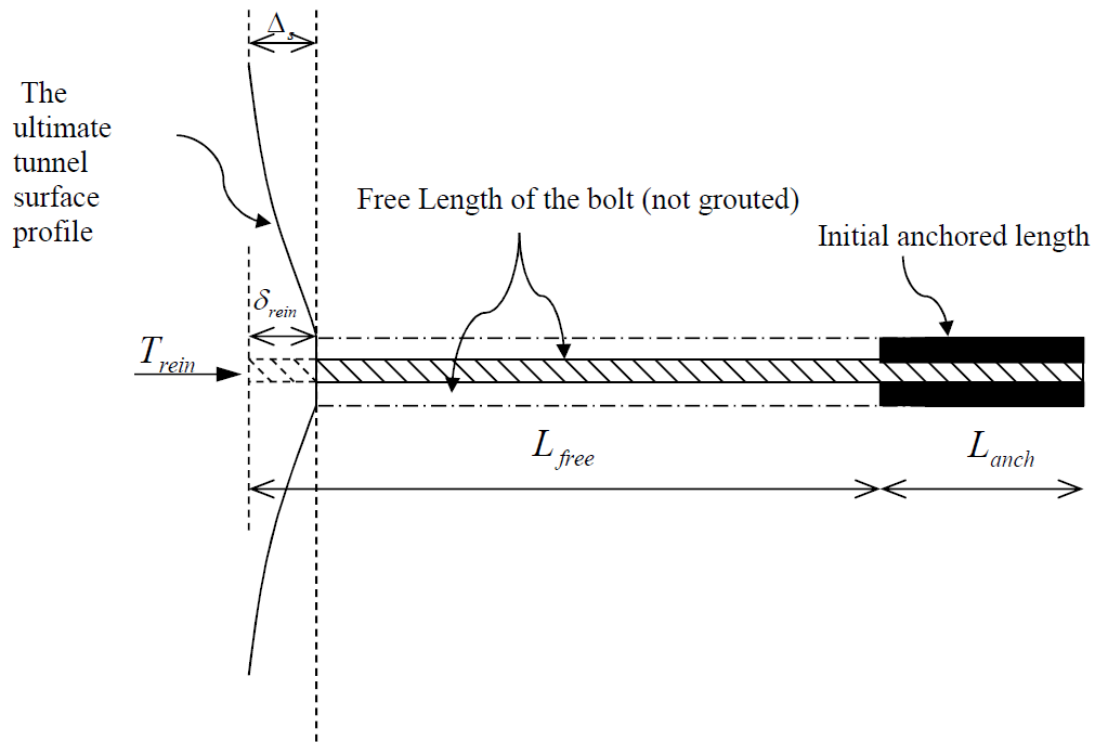
790

791

792

793

794

795

796

(a)

Tunnel surface deformation after the excavation

Tunnel surface at the Excavation stage

The ultimate tunnel surface profile

δ_b

Rock bolt elongation

Rockbolt

Rock mass surrounding the bolt

(b) Δ_s

The ultimate tunnel surface profile

Tunnel surface at the Excavation stage

Rockbolt

δ_{rain} δ_b

Rock bolt elongation

Tunnel surface deformation after the excavation

797

798   Figure 2. Rock mass and bolt interaction at tunnel surface in (a) ideal connection and

799   (b) real connection between the bolt and rock mass

800

801

802

Figure 3. Total reduction of bolt elongation
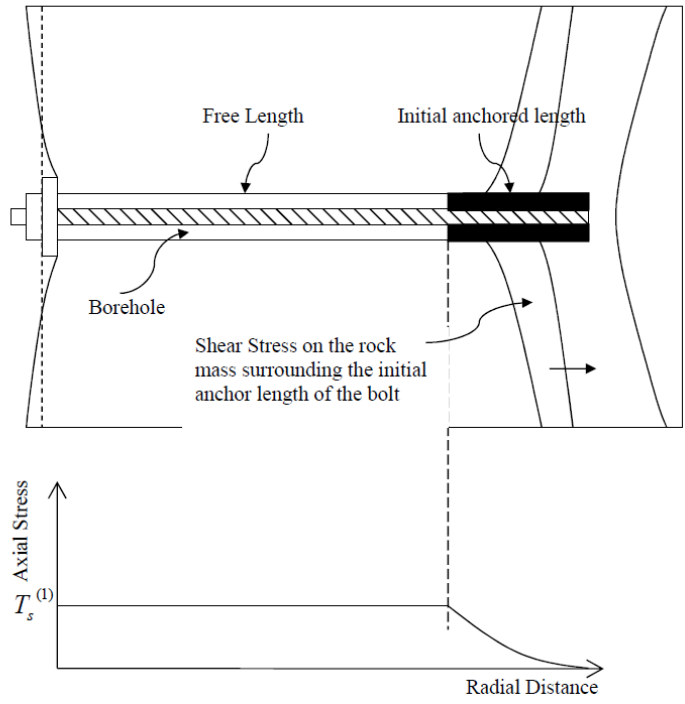
803

804

805

806

807
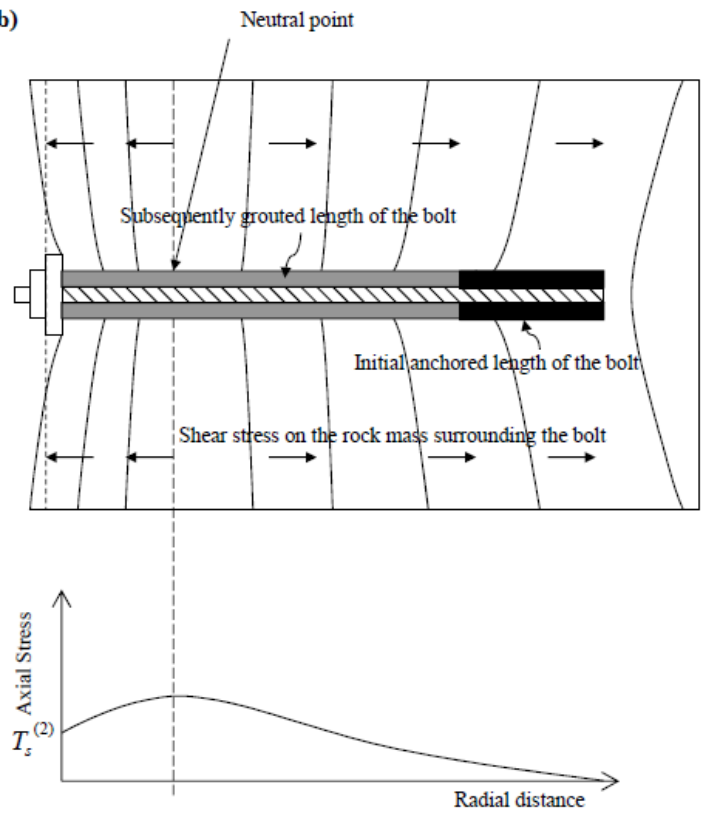
808

809

810

811

812

813

814

815

816

(a)

Free Length   Initial anchored length

Borehole

Shear Stress on the rock
mass surrounding the initial
anchor length of the bolt

Axial Stress

$T_s^{(1)}$

Radial Distance

817

(b)

Neutral point

Subsequently grouted length of the bolt

Initial anchored length of the bolt

Shear stress on the rock mass surrounding the bolt

Axial Stress

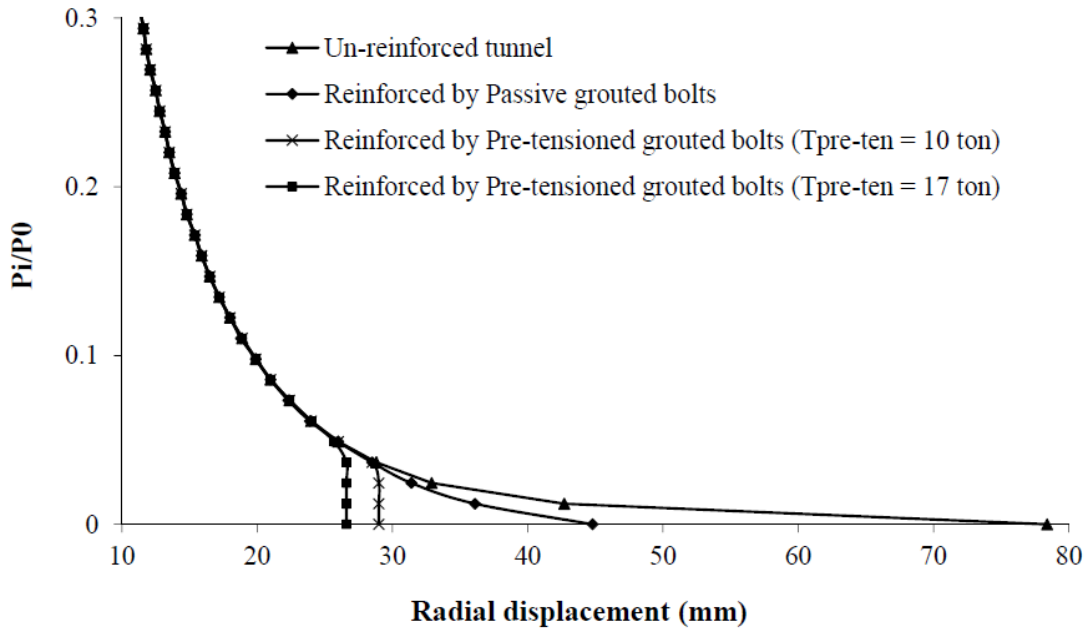$T_s^{(2)}$

Radial distance

818

42

819   Figure 4. Interaction of bolt with its surrounding rock mass for *Case B*. Loading

820   mechanism of the bolt (a) for the first step (b) for the second step
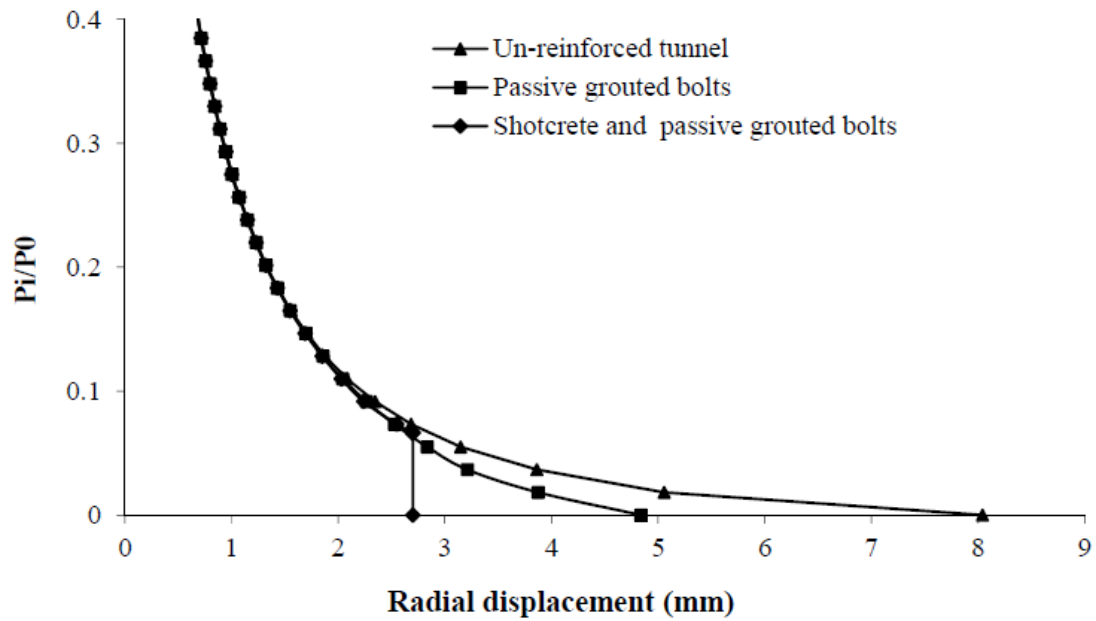
821

822   Figure 5. Ground response curves for the rock mass around Kielder Experimental

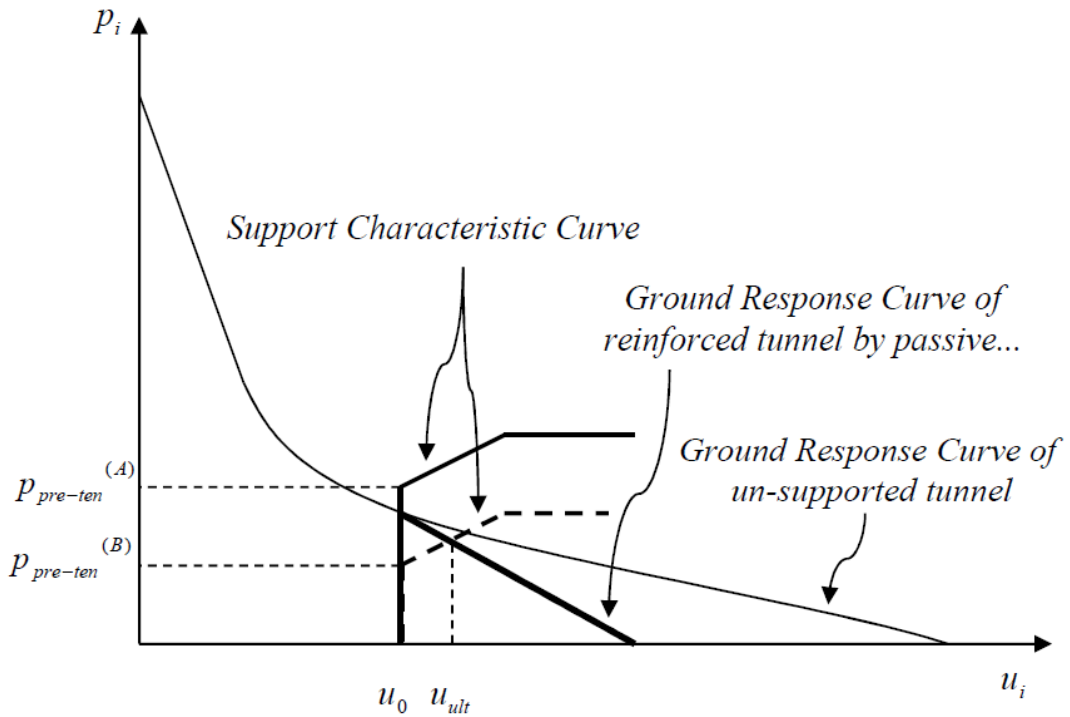823   Tunnel (Example 1) in the rockbolted and rockbolt with shotcreted section

824

825

826   Figure 6. Ground response curve for the rock mass around tunnel in Examples 2 for
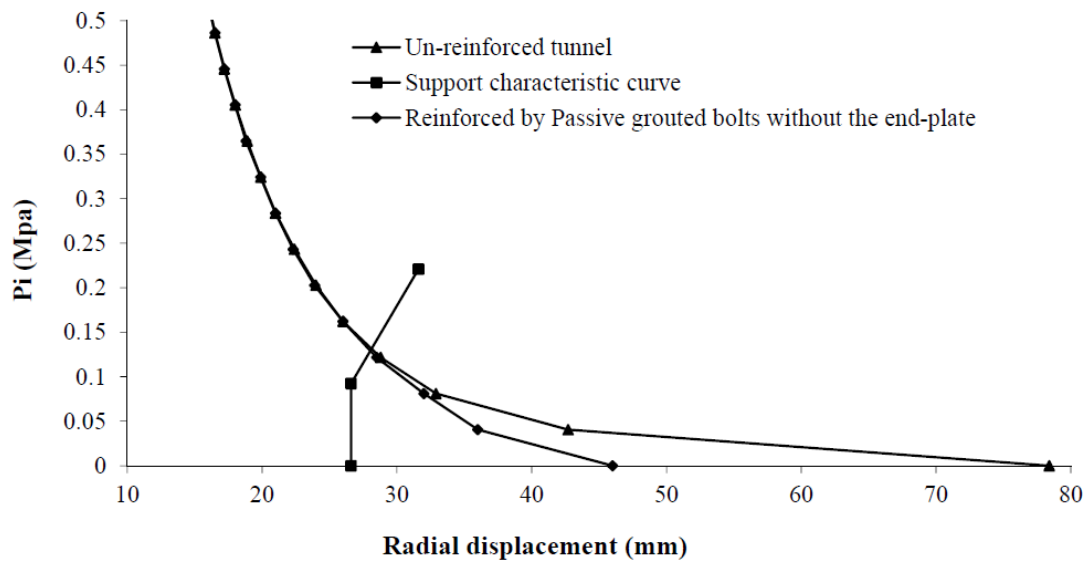
827   *Case A* and *Case B*

828

829

830   Figure7. Un-grouted pre-tensioned characteristic curve (solid line for *Case A*

44

831   condition and dashed line for *Case B* condition) and ground response curves of un-

832   supported tunnel and reinforced by passive grouted bolts

833

834   Figure 8. Un- grouted pre-tensioned characteristic curve and the ground response

835   curves of tunnel for un-reinforced and reinforced by passive grouted bolts (Example 2

836   by simple practical method)
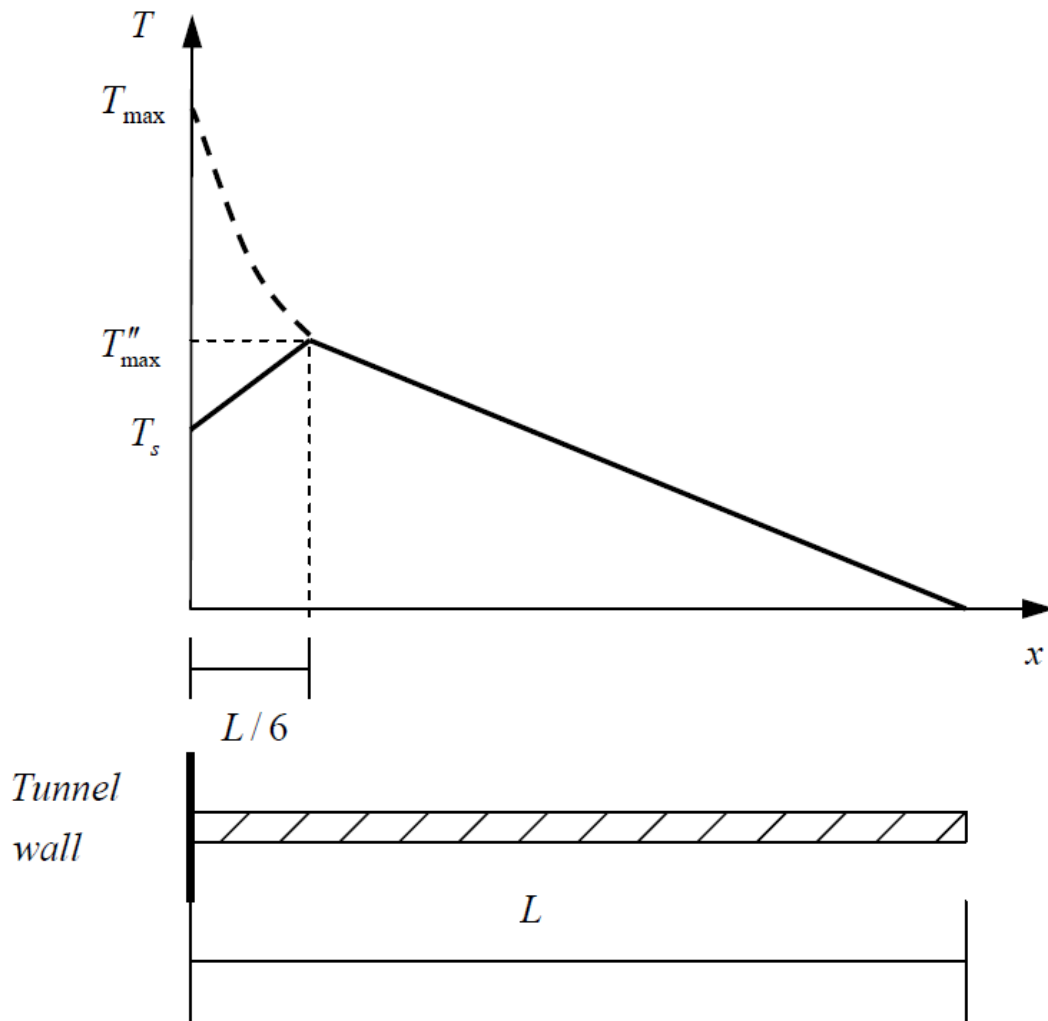
837

838

839

840

841

842

843

844

845

846

847

848

849

850   Figure 9. Simplified graphic of force along the bolt (two solid line by Oreste (2008)

851   and dashed curve by Ranjbarnia (2014))

852

853

854

855

856

857

858

859

860 **Table 1.** Mechanical properties of mudstone in the Kielder Experimental Tunnel (data

861 from Freeman 1978; Hoek and Brown 1980)

Parameter	Value
Axial compressive strength σ_c (MPa)	37
Tunnel radius, r_i (m)	1.65
In-situ stress, p_0 (MPa)	2.56
Deformation modulus, E_m (MPa)	5000
Poisson's ratio, ν	0.25
Peak Strength parameter, m_p	0.1
Peak Strength parameter, s_p	0.00008
Residual Strength parameter, m_r	0.05
Residual Strength parameter, s_r	0.00001
Dilation angle (degree), ψ	10
Strain softening parameters*, gradients of $-\varepsilon_3^p$ vs. ε_1^p lines in the residual stage, f	1.1
Strain softening parameters*, gradients of $-\varepsilon_3^p$ vs. ε_1^p lines in the softening stage, h	1.2
Strain softening parameters*, constant defining strain at which residual strength is reached, μ	7.5

862 *these parameters were computed by the authors from the value of dilation angle

863

864

865

866

867

868

869

870

871

47

872   **Table 2.** Geometrical parameters of passive grouted rockbolts and shotcrete in the

873   Kielder Experimental Tunnel (data from Ward et al. 1976; Freeman 1978; Hoek and

874   Brown 1980)

Parameter	Value
Rockbolt Length, $L\ (m)$ *	1.8
Initial anchored length, $L_{anch}\ (m)$	0.5
Young's modulus of rockbolt, $E_s\ (GPa)$	210
Bolt diameter, $d_b\ (mm)$	20
Borehole diameter, $d_g\ (mm)$ **	60
Distance between rockbolt, $S_l \times S_c\ (m \times m)$	0.9*0.9
Early age Young's modulus of shotcrete, $E_{shot}\ (GPa)$	2
Shotcrete thickness, (mm)	140
Bolt head stiffness, $K_s\ (MN)$ ***	320
Shotcrete pressure on the tunnel surface (MPa) ****	0.17

875   * According to Hoek and Brown (1980) study, this value was smaller than what was required. Authors

876   of this paper used the required value.

877   ** assumed typical value

878   ***calculated by the authors for the shotcreted section of tunnel where perfect constrained was

879   predicted for the end plate of bolt.

880   **** calculated by the authors from the classic formula presented by Hoek and Brown (1980).

881   Shotcrete layer radial deformation was 1.5 mm.

882

883   Table 3. Calculated and measured deformations (data from Stille et al. 1989) at the

884   rock surface for reinforced and un-reinforced rock mass

Parameter	Measured (mm)	Calculated* (mm)
Un-reinforced tunnel	8	8.05
Passive grouted bolt section	4-5	4.84
Passive grouted bolt and Shotcrete section	2-3	2.7

885   *By authors

886

887

888   Table 4. The output results of Example 2

Example		Ultimate convergence (mm)	Plastic radius (mm)
Un-reinforced tunnel		78.4	12.27
Reinforced tunnel	by the passive bolts	44.8	9.37
	by the pre-tensioned bolts (Case A)	26.6	8.1
	by the pre-tensioned bolts (Case B)	29.8	8.42

889

890

891

892   Table 5. The input and output data of Example 2 calculated by simple practical

893   method

Parameter	Value
σ_{r_0-pre} (Mpa)*	0.0924
ξ	1.2
k_{sys} (MN/m^3)	25.7
u_1 (mm)	26.6
u_{ult} (mm)	28.5

894   *Calculated by $p_{pre-ten} = T_s / C_0$ where T_s is obtained by Eq. (33)

895

896